Short Communication

Synthesis of Spinel ZnMn$_2$O$_4$ Nanoparticle Assemblies Via a Flower-like ZnO Precursor Route for Lithium Battery Anodes with Enhanced Electrochemical Performance

LinLin Wang[1,2,], ZhiPeng Wu[1], Kaibin Tang[2], XiaoZhu Zhang[1], Min Zhang[1], DaoLi Zhao[3], Jingli Xu[1,*]*

[1]College of Chemistry and Chemical Engineering, Shanghai University of Engineering Science, 333 Longteng Road,Shanghai 201620, P. R. China
[2]Department of Chemistry, University of Science and Technology of China, Hefei 230026, P.R. China
[3]Department of Chemistry, University of Cincinnati, Cincinnati, OH, 45221-0172, USA
[*]E-mail: wlinlin@mail.ustc.edu.cn; xujingli@sues.edu.cn

In this work, the spinel ZnMn$_2$O$_4$ nanoparticle assemblies have been successfully prepared using a flower-like ZnO as a precursor via a facile a water bath method. The method is a low-cost, simple and large-scale production. The electrochemical performance as Li-ion battery (LIB) materials was tested, the ZnMn$_2$O$_4$ nanoparticle assemblies exhibit a high reversible capacity of 500 mA h g^{-1} for 150 cycles at 500 mA g^{-1}. Even at high rate of 1600 mA g^{-1}, the ZnMn$_2$O$_4$ can still retain a stable capacity of 235 mAh g^{-1}. These results suggest that the facile synthetic strategy of preparing the ZnMn$_2$O$_4$ nanoparticle assemblies can improve electrochemical performance with higher-rate capability and better cycle durability.

1. INTRODUCTION

With stoichiometric or non-stoichiometric compositions, A$_x$B$_{3-x}$O$_4$ (A, B= Mn, Zn, etc.) are typically in a spinel structure, which have been developed as promising anode materials for LIBs [1-3]. Of particular note, the spinel structure has much better interesting physical and chemical properties. When they are used as an anode material, the features of the complex chemical and their synergies can contribute to the extra electrochemical capacity, causing they can deliver a high reversible capacity. Furthermore, it is useful to obtain the interesting and highly tunable properties that different valences of the cations present in the spinel mixed transition-metal oxides systems [2, 4-6]. For instance, as a

typical spinel structure, $ZnMn_2O_4$ has tetrahedral and octahedral gaps of oxygen sublattices, and the center is Zn^{2+} and Mn^{3+} ions, respectively (Fig. 1). Tetrahedral ZnO_4 groups are established by Zn^{2+} with neighboring O^{2+} and octahedral site MnO_6 groups are established by Mn^{3+} with neighboring O^{2+} (Fig. 1) [7,8]. Among these AB_2O_4 series, $ZnMn_2O_4$ can be a competitive candidate due to its much cheaper, environmentally friendly, and lower operating voltage (average discharge/charge voltages of 0.5 V/1.2 V, respectively) than that of the Fe or Co oxides [9-11].

Recently, various methods have been developed to obtain $ZnMn_2O_4$ materials with much different morphologies. For example, Song and co-workers reported nanocrystalline $ZnMn_2O_4$ is synthesized by a polymer-pyrolysis method with a reversible capacity of 569 mA h g^{-1} after 50 cycles at 100 mA h g^{-1} [9]. Abu-Lebdeh et al. reported $ZnMn_2O_4$ nanoparticles prepared by a hydrothermal synthesis at 160 ^{o}C using ethylene glycol as a solvent, and then prepared $ZnMn_2O_4$ electrodes with a stable capacity of 430 mA h g^{-1} for 100 cycles at 0.1 C [12]. The $ZnMn_2O_4$ nanoplate assemblies fabricated by thermal transformation of metal–organic nanoparticles into metal–oxide nanoparticles and demonstrated the reversible discharge capacity of 578 mA h g^{-1} up to 30 cycles at 60 mA h g^{-1} [13]. From these examples, we found that above strategies methods for preparing $ZnMn_2O_4$ either carried out a relatively complex or required toxic raw material or solvent, limiting their application development. Based on above cases; obviously, there is much room for improvement of electrochemical performance of $ZnMn_2O_4$ electrode, especially in high rates, by rationally design or tuning the morphologies of $ZnMn_2O_4$ structure.

In this work, $ZnMn_2O_4$ nanoparticles congeries with micron size was successfully synthesized in a gram scale using a flower-like ZnO as a precursor via a facile a water bath method. The electrode performance of the sample was electrochemically investigated, which exhibits a reversible and stable capacity of 500 mAh g^{-1} up to 150 cycles at 500 mA g^{-1} and also reaches a stable capacity of 235 mA h g^{-1} at 1600 mA g^{-1}.

2. EXPERIMENTAL

2.1. Sample preparation

2.1.1. Preparation of ZnO

ZnO precursor was prepared using our previous reported method [14]. $ZnCl_2{\cdot}5H_2O$ (10.0 mmol) and $C_6H_8O_7{\cdot}H_2O$ (6.7 mmol) were added into distilled water (10 mL), then NaOH (50.0 mmol) was added into above solution. Then, put into 40 mL water and we prepared a precursor solution about ten min. The precipitate was washed and dried.

2.1.2. Preparation of $ZnMn_2O_4$

ZnO (1.0 mmol) was dissolved in deionized water (50 mL), mixed with $Mn(Ac)_2{\cdot}4H_2O$ (2.0 mmol) and the reaction was stirred at room temperature. Then, the obtained solution was heated with

continuous stirring at 70 ^{o}C for 24 h in round-bottomed flask. Then, the precipitate was harvested by centrifugation, washed and dried. Last, the obtained product was calcined in air as 350 ^{o}C for 3 h and the $ZnMn_2O_4$ was obtained.

2.2. Characterization

The samples were characterized by X-ray powder diffraction (XRD) (Philips X'pert X-ray diffractometer equipped with Cu Kα radiation). The morphologies of the samples were observed by field-emission scanning electron microscopy (FESEM, JEOL JSM-6700F).

2.2. Electrochemical Performance

The working electrode consisted of 65 wt % $ZnMn_2O_4$, 25 wt % acetylene black and 15 wt % polyvinylidene fluoride (PVDF). The 2016 coin cells were assembled in Ar-filled glove box using metallic lithium foil as the anode, Celgard 2600 as the separator and 1 M $LiPF_6$ (dissolved in ethylene carbonate and dimethyl carbonate with a 1:1 volume ratio). The electrochemical tests were performed on a LAND-CT2001 battery cycler (Wuhan, China) testing system in the voltage range of 0.01–3.0 V (vs. Li/Li^+).

3. RESULTS AND DISCUSSION

3.1. Crystal structure and morphology in the XRD pattern of the typical sample

XRD pattern of the as-prepared sample was shown in Fig. 2. All the diffraction peaks (Fig.2) can be assigned to the standard tetragonal $ZnMn_2O_4$ (JCPDS file No.71-2499, space group $I4_1$/amd) and no additional peaks are found, indicating that it is pure $ZnMn_2O_4$.
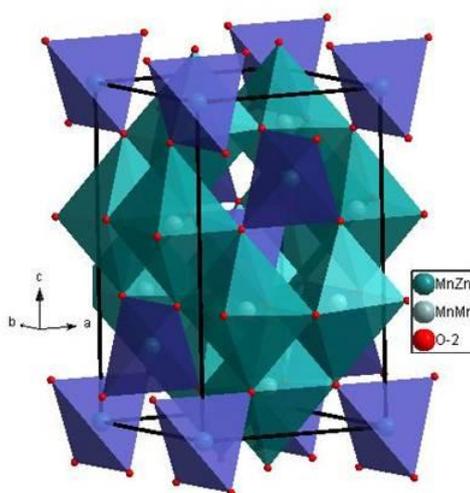

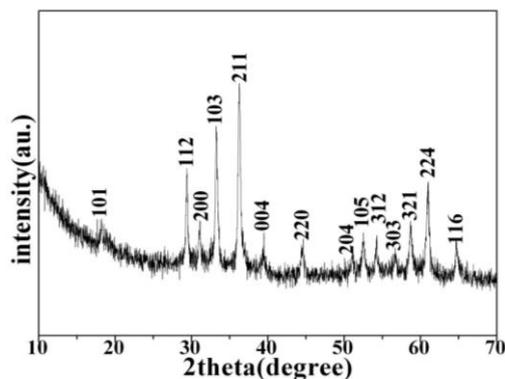**Figure 1.** Crystal structure of $ZnMn_2O_4$.

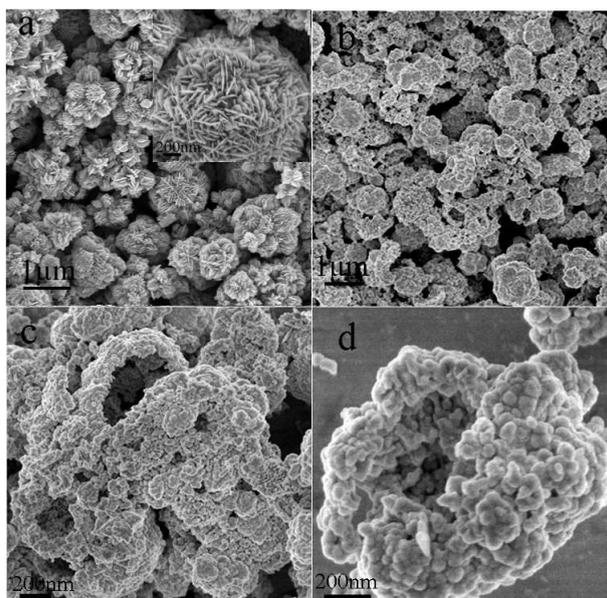**Figure 2.** XRD pattern of ZnMn$_2$O$_4$ sample.

Figure 3. (a) SEM image of ZnO precursor; (b-d) SEM images of the ZnMn$_2$O$_4$ sample obtained in a typical synthesis: (b) low magnification, (c) high magnification, (d) a single congery.

The morphology of the ZnO precursor and the as-prepared ZnMn$_2$O$_4$ powder were studied by SEM and the images of the sample are shown in Fig. 3a and Fig. 3b-d, respectively. The ZnO precursor is nanosheets-assembled flower (Fig. 3a). From Fig. (3b-d), it is observed that ZnMn$_2$O$_4$ looks like nanoparticle congeries with micron sizes. After magnification, some sphere-shaped congeries show the cavity and they are formed of amounts of nanoparticles with average diameters ~ 80 nm (Fig. 3c-d).The small primary nanoparticles and these cavities help to short the Li$^+$ diffusion path, thus improving the electrochemical property of ZnMn$_2$O$_4$. The overall schematic model of the synthetic procedure is presented in Fig. 4. Meanwhile, the commercial ZnO is used to obtain of ZnMn$_2$O$_4$. The morphologies of the corresponding ZnMn$_2$O$_4$ are mixture of nanorods, and nanoparticles with a broad size distribution, as well as the irregular shapes (Fig. 5a and b). By the experimental investigations, we found that the morphologies of the ZnO precursor control the final product shapes.
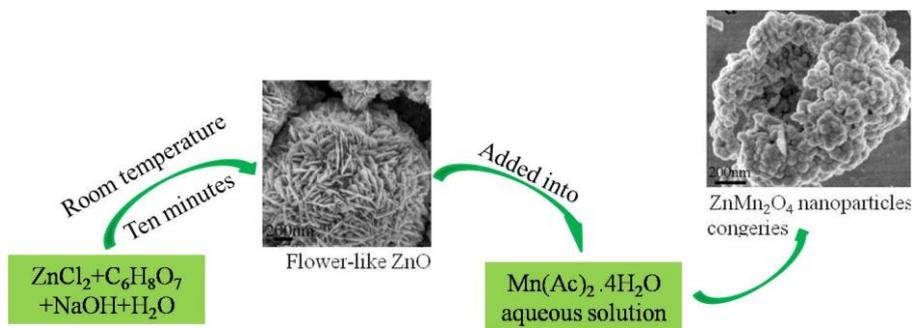
Figure 4. Schematic showing the synthetic route of the ZnMn$_2$O$_4$ nanoparticles congeries.
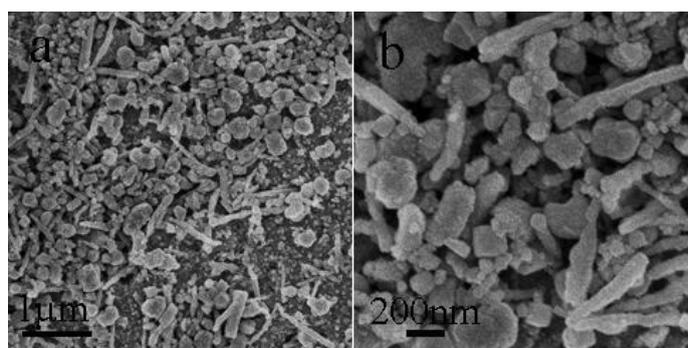

Figure 5. SEM images: (a) low magnification of the ZnMn$_2$O$_4$ prepared with commercial ZnO, (b) high magnification of the ZnMn$_2$O$_4$ prepared

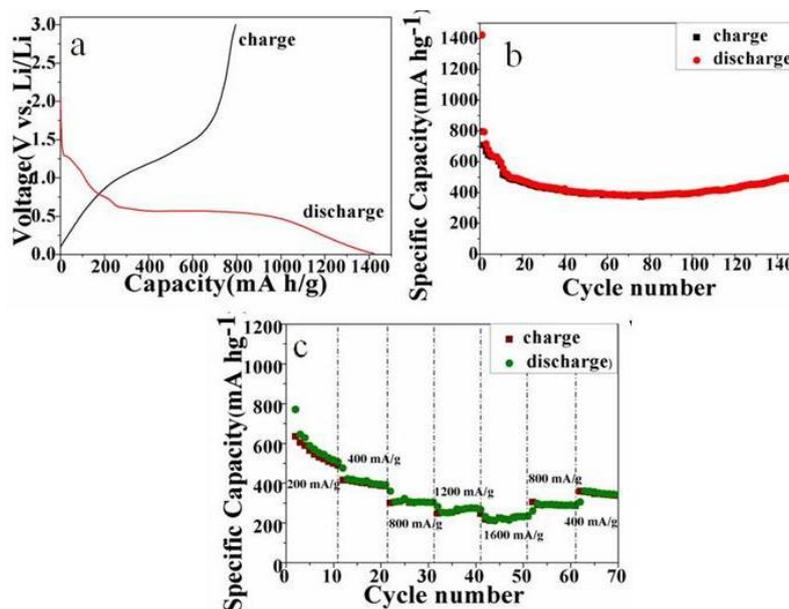## 3.2. Electrochemical performance

Figure 6. (a) First discharge/charge curves for the ZnMn$_2$O$_4$ at 500 mA g^{-1}; (b) Discharge capacity and Coulombic efficiency of the composite for the 150 cycles at 500 mA g^{-1}; (c) Rate capability of ZnMn$_2$O$_4$ electrode at different current densities.

The electrochemical properties of $ZnMn_2O_4$ particles congeries are investigated by a galvanostatic method. Fig. 6a shows first galvanostatic discharge–charge curves for $ZnMn_2O_4$ nanoparticles electrode at a current rate of 500 mA g^{-1}, which exhibit two voltage plateaus of ~1.25, and ~0.5 V for the first discharge curves. It corresponds to a multi-step electrochemical reaction of $ZnMn_2O_4$ related to the reduction of Mn^{3+} to Mn^{2+}, and Zn, Mn and zinc-lithium alloy were formed, as discussed in the literature [15]. The $ZnMn_2O_4$ nanoparticles congeries reaches the first discharge capacity of 1422 mA h g^{-1} and charge capacity of 794 mA h g^{-1}, respectively, indicating a coulombic efficiency of 56%. Fig. 6b shows the cycling performances and columbic efficiency of the $ZnMn_2O_4$ nanoparticles congeries at a 500 mA g^{-1}. After 150 cycles, $ZnMn_2O_4$ exhibits a high discharge (a reversible) capacity of 500 mAh g^{-1} and columbic efficiency is over 99% $ZnMn_2O_4$ after the second cycle. Fig. 6c shows rate capability of the $ZnMn_2O_4$ electrodes at 200 mA g^{-1}, 400 mA g^{-1}, 800 mA g^{-1} and 1600 mA g^{-1}. It delivers a specificity capacity of 507 mA h g^{-1} obtained at 200 mA g^{-1}after 11 cycles, and this value is decreased to 390, 305, 267 mA h g^{-1} at current densities of 400, 800 and 1200 mA g^{-1}, respectively. Even at a current density of 1600 mA g^{-1}, the reversible capacity of the $ZnMn_2O_4$ nanoparticles also remains at 235 mA h g^{-1}. Additionally, as the current density is switched back to 800 and 400 mA g^{-1}, the reversible capacity is able to return to 290 and 340 mA h g^{-1} The good cyclability and rate capability of the $ZnMn_2O_4$ nanoparticle-assembled sphere-shaped congeries material is might be reasonable to related to the structural features. Firstly, the hollow interior may buffer the volume variation during discharge/charge process, thus stabilizing the structure [16-18]; Secondly, it can also facilitate the electrolyte penetration and increase the contact area between the electrode and electrolyte and shorten the Li^+ diffusion path [16-18]. Thirdly, they are formed of amounts of nanoparticles and t the nanoparticles can enhanced the electron transport within the particle and provide a high contact area with the electrolyte etc.[19]. The above-mentioned structural features give rise to the conversion reaction of $ZnMn_2O_4$ nanoparticles assemblies have better reversibility and further causing the electrochemical performance to enhance [20]. Furthermore, it provides a feasible strategy to design $ZnMn_2O_4$ anode materials.

4. CONCLUSION

The $ZnMn_2O_4$ sphere-shaped congeries with micron size we successfully synthesized using a flower-like ZnO as a precursor via a facile a water bath method. It provides a facile, effective method to obtain $ZnMn_2O_4$ structure. The as-prepared nanoparticle-assembled $ZnMn_2O_4$ congeries were used as anode materials for LIBs, which shows good stability and high rate performance, superior to these of some reported $ZnMn_2O_4$ anodes. The excellent electrochemical performance of the $ZnMn_2O_4$ material could be attributed to nanoparticle-assembled $ZnMn_2O_4$ congeries with hollow interior, which can which favors fast diffusion of electrolyte and offering buffer space for the volume change and retaining high structural stability during reversible electrochemical process, and the advantage of using nanoparticles can also be beneficial to improve the electrochemical properties.

References

1. L. Zhou, D. Zhao, X. W. Lou, *Adv. Mater*. 24(2012) 745-748.
2. C. Z. Yuan, H. B. Wu, Y. Xie, X. W. Lou, *Angew. Chem. Int. Ed.* 52(2013) 2-19.
3. B. Liu, J. Zhang, X. Wang, G. Chen, D. Chen, C. Zhou, G. Shen, *Nano Lett.* 12(2012) 3005-3011.
4. G. B. Zeng, N. Shi, M. Hess, X. Chen, W. Chen, T. X. Fang, M. Niederberger, *ACS nano*. 9(2015) 4227-4235.
5. L. Hu, L.Wu,M. Liao, X. Hu, X. Fang, *Adv. Funct. Mater.* 22(2012), 998-1004
6. F. Cheng, J. Shen, B. Peng, Y. Pan, Z. Tao, J. Chen, *Nat. Chem*. 3(2011),79-84.
7. N. Bahlawane, P. H. T. Ngamou, V. Vannier, T. Kottke, J.Heberle, K. Kohse-Hoeinghaus, *Phys. Chem. Chem. Phys.* 11(2009) 9224-9232.
8. H. Li, B. Song, W. J. Wang, X. L. Chen, *Mater. Chem. Phys*. 130 (2011) 34-44.
9. Y. Yang, Y. Zhao, L. Xiao, L. Zhang, *Electrochim. Comm*., 10(2008)1117-1120.
10. P. F. Teh, Y. Sharma, Y. W. Ko, S. S. Pramana, M. Srinivasan, *RSC Adv*., 3(2013) 2812-2821.
11. Y. Deng, S. Tang, Q. Zhang, Z. Shi, L. Zhang, S. Zhan, G. Chen, *J. Mater. Chem*., 21(2011) 11987-11995.
12. F. M. Courtel, Y. Abu-Lebdeh, I. J. Davidson, *Electrochim. Acta*, 71(2012) 123-127.
13. J. Zhao, F. Wang, P. Su, M. Li, J. Chen, Q. Yang, C. Li, *J. Mater. Chem*., 22(2012) 13328-13333.
14. L. L. Wang, D. L. Zhao, M. Zhang, C. H. Wang, K. K. Tang, X. Z. Zhang, J. L. Xu, *Nano LIFE*, 4 (2014) 1441015 (7 pages).
15. Z. Bai, N. Fan, C. Sun, Z. Ju, C. Guo, J. Yang, Y. Qian, *Nanoscale*, 5(2013) 2442-2447.
16. X. F. Chen, L. Qie, L. L. Zhang, W. X. Zhang, Y. H. Huang, *J. Alloys. Compds*, 559(2013) 5-10.
17. G. Q. Zhang, L. Yu, H. E. Hostera, X. W. Lou, *Nanoscale*, 5(2013) 877-881.
18. J. Wang, Y.C. Liu, S.Y. Wang, X.T. Guo, Y. P. Liu, *J. Mater. Chem. A*, 2014, 2, 1224-1229
19. P. G. Bruce, B. Scrosati, J. M. Tarascon, *Angew. Chem. Int. Ed.* 47(2008) 2930-2946.
20. L. L. Wang, H. X. Gong, C. H. Wang, D. K. Wang, K. B. Tang, Y. T. Qian, *Nanoscale*, 4(2012) 6850-6855.